

# Lead-Free Halide Double Perovskites via Heterovalent Substitution of Noble Metals.

George Volonakis,<sup>†,¶</sup> Marina R. Filip,<sup>†,¶</sup> Amir Abbas Haghhighirad,<sup>‡</sup> Nobuya Sakai,<sup>‡</sup>  
Bernard Wenger,<sup>‡</sup> Henry J. Snaith,<sup>\*,‡</sup> and Feliciano Giustino<sup>\*,†</sup>

*Department of Materials, University of Oxford, Parks Road OX1 3PH, Oxford, UK, and  
Department of Physics, University of Oxford, Clarendon Laboratory, Parks Road, Oxford OX1  
3PU, UK*

E-mail: feliciano.giustino@materials.ox.ac.uk; henry.snaith@physics.ox.ac.uk

---

\*To whom correspondence should be addressed

<sup>†</sup>Department of Materials, University of Oxford

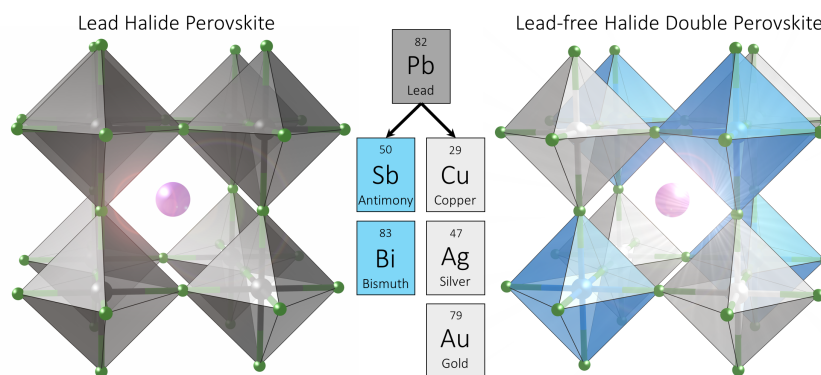
<sup>‡</sup>Department of Physics, University of Oxford

<sup>¶</sup>These authors contributed equally to this work

## Abstract

Lead-based halide perovskites are emerging as the most promising class of materials for next generation optoelectronics. However, despite the enormous success of lead-halide perovskite solar cells, the issues of stability and toxicity are yet to be resolved. Here we report on the computational design and the experimental synthesis of a new family of Pb-free inorganic halide double-perovskites based on bismuth or antimony and noble metals. Using first-principles calculations we show that this hitherto unknown family of perovskites exhibits very promising optoelectronic properties, such as tunable band gaps in the visible range and low carrier effective masses. Furthermore, we successfully synthesize the double perovskite  $\text{Cs}_2\text{BiAgCl}_6$ , we perform structural refinement using single-crystal X-ray diffraction, and we characterize its optical properties via optical absorption and photoluminescence measurements. This new perovskite belongs to the  $Fm\bar{3}m$  space group, and consists of  $\text{BiCl}_6$  and  $\text{AgCl}_6$  octahedra alternating in a rock-salt face-centered cubic structure. From UV-Vis and PL measurements we obtain an indirect gap of 2.2 eV. The new compound is very stable under ambient conditions.

### Table of Contents Image



**Keywords:** Noble-metal halide double perovskites, Lead-free perovskites, Computational design, materials synthesis, structure refinement, UV-Vis spectra, Photoluminescence spectra

Perovskites are among the most fascinating crystals, and play important roles in a variety of applications, including ferroelectricity, piezoelectricity, high- $T_c$  superconductivity, ferromagnetism, giant magnetoresistance, photocatalysis and photovoltaics.<sup>1-8</sup> The majority of perovskites are oxides and are very stable under ambient temperature and pressure conditions.<sup>4,9</sup> However, this stability is usually accompanied by very large band gaps, therefore most oxide perovskites are not suitable candidates for optoelectronic applications. The most noteworthy exceptions are the ferroelectric perovskite oxides related to  $\text{LiNbO}_3$ ,  $\text{BaTiO}_3$ ,  $\text{Pb}(\text{Zr}, \text{Ti})\text{O}_3$  and  $\text{BiFeO}_3$ , which are being actively investigated for photovoltaic applications, reaching power conversion efficiencies of up to 8%.<sup>9</sup> The past five years witnessed a revolution in optoelectronic research with the discovery of the organic-inorganic lead-halide perovskite family. These solution-processable perovskites are fast becoming the most promising materials for the next generation of solar cells, achieving efficiencies above 20%.<sup>10-13</sup> Despite this breakthrough, hybrid lead-halide perovskites are known to degrade due to moisture and heat,<sup>14</sup> upon prolonged exposure to light,<sup>15</sup> and are prone to ion or halide vacancy migration, leading to unstable operation of photovoltaic devices.<sup>16,17</sup> At the same time the presence of lead raises concerns about the potential environmental impact of these materials.<sup>18,19</sup> Given these limitations, identifying a stable, non-toxic halide perovskite optoelectronic material is one of the key challenges to be addressed in the area of perovskite optoelectronics.

The starting point of our search for a lead-free halide-perovskite is the prototypical inorganic compound of the family  $\text{CsPbI}_3$ .  $\text{CsPbI}_3$  is an  $\text{ABX}_3$  perovskite where the heavy metal cations  $\text{Pb}^{2+}$  and the halide anions  $\text{I}^-$  occupy the B and X sites, respectively, while  $\text{Cs}^+$  occupies the A site. The most obvious route to replacing Pb in this compound is via substitution of other group-14 elements such as Sn and Ge. However both elements tend to undergo oxidation, for example from  $\text{Sn}^{2+}$  to  $\text{Sn}^{4+}$ , leading to a rapid degradation of the corresponding halide perovskites.<sup>20-23</sup> More generally, it should also be possible to substitute lead by other divalent cations outside of group-14 elements. However, our previous high-throughput computational screening of potential candidates showed that the homovalent substitution of lead in halide perovskites impacts negatively the optoelectronic properties by increasing band gaps and effective masses.<sup>24</sup>

Another possible avenue is to consider heterovalent substitution, that is the formation of a double perovskite structure with a basic formula unit  $A_2BB'X_6$ .<sup>4</sup> This type of compounds are abundant in the case of oxides and are well known for their ferroelectric, ferromagnetic and multi-ferroic properties.<sup>4</sup> Additionally, double perovskites have been explored in order to tune the band gap of oxide perovskites.<sup>25,26</sup> On the other hand, halide double perovskites remain a much less explored class of materials. To date, the best known halide double perovskites are based on alkali and rare-earth metals, and are investigated for applications as scintillators in radiation detectors.<sup>27</sup>

In order to replace the divalent Pb cations and maintain the total charge neutrality, the  $B'$  and  $B''$  sites have to be occupied by one monovalent and one trivalent cation. We search for our  $B'^{3+}$  metallic cations among the pnictogens, and consider Bi and Sb as the most suitable choices. Arsenic is less desirable owing to its toxicity. For the monovalent cations we choose the noble metals Cu, Ag and Au. From elementary considerations Cu, Ag, and Au appear very promising for optoelectronic applications. In fact, in their metallic form, the noble metals are the best known electrical conductors, owing to their filled  $d^{10}$  shell and the free-electron-like behaviour of the  $s^1$  shell. In addition, in an octahedral environment, the ionic radii of  $Cu^+$  (0.91 Å),  $Ag^+$  (1.29 Å) and  $Au^+$  (1.51 Å) are similar to those of  $Pb^{2+}$  (1.19 Å),  $Sb^{3+}$  (0.76 Å) and  $Bi^{3+}$  (1.03 Å).<sup>28</sup> Following this simple reasoning we investigate hypothetical halide double perovskites with the pairs  $B'/B''$  where  $B' = Sb, Bi$ , and  $B'' = Cu, Ag, Au$ .

We investigate the electronic properties of these hypothetical compounds from first principles using density functional theory (DFT) in the local density approximation (LDA). We construct ‘rock-salt’ double perovskites, whereby  $B'$  and  $B''$  alternate in every direction (shown in Figure 1a). The rock-salt ordering is known to be the ground state for most oxide double perovskites,<sup>4</sup> therefore it can be expected to hold also in the present case. For each model structure we perform full structural optimization using DFT-LDA and calculate the electronic band gaps using the hybrid PBE0 functional as described in the Supporting Information.

In Figure 1b-c we show a comparative view of the band gaps calculated for the entire  $Cs_2B'B''X_6$  family. We find that all band gaps are below 2.7 eV, spanning the visible and near infrared optical

spectrum. The band gaps are indirect and increase as we move up the halogen or the pnictogen column in the periodic table, but do not follow a monotonic trend with respect to the size of the noble metal cation. This behaviour can be explained by the character of the electronic states at the band edges. Indeed, as shown in Figure S1 of the Supporting Information, the conduction band bottom and valence band top in each case are predominantly of pnictogen- $p$  and halogen- $p$  character, respectively. As we move up in the periodic table the energy of the halogen- $p$  states decreases, thus lowering the energy of the valence band top. Similarly, the energy of the pnictogen- $p$  states decreases when moving up in the periodic table, thus lowering the energy of the conduction band bottom. The electron and hole effective masses calculated at the band edges exhibit an anisotropic behaviour in most cases (see Table S1). Throughout the entire family of compounds the electron masses are more isotropic than the hole masses. For clarity, in Figure 1 we report the transport effective masses,<sup>29</sup> as defined in the Supporting Information. We note that all compounds exhibit small carrier effective masses between 0.1 and 0.4  $m_e$ , very close to those calculated for  $\text{CH}_3\text{NH}_3\text{PbI}_3$  within the same level of theory.<sup>30</sup>

The electronic band structures of these halide double perovskites (shown in Figure S2 and S3) exhibit several features of particular interest. In all cases, the valence band maximum (VBM) is at the  $X$   $(0,0,2\pi/a)$  point in the Brillouin zone. The conduction band minimum (CBM) is at  $\Gamma$   $(0,0,0)$  for  $\text{Cs}_2\text{BiAgCl}_6$ ,  $\text{Cs}_2\text{BiCuCl}_6$  and  $\text{Cs}_2\text{BiCuBr}_6$ , while for the other compounds the CBM is at the  $L$   $(\pi/a, \pi/a, \pi/a)$  point. The FCC cubic crystals of the former three compounds are indirect band gap semiconductors, however a small disturbance of the conventional unit cell symmetry could render the direct optical transition allowed. This is shown in Figure S4, where the band structure of  $\text{Cs}_2\text{BiAgCl}_6$  is calculated in the conventional unit cell (which corresponds to two primitive cells). Here, as a result of Brillouin zone folding in the conventional FCC unit cell, the band gap of  $\text{Cs}_2\text{BiAgCl}_6$  becomes direct at the  $\Gamma$  point. In practice, this effect could be realized by incorporating an organic cation, like methylammonium ( $\text{CH}_3\text{NH}_3^+$ ) or formamidinium ( $\text{CHN}_2\text{H}_4^+$ ) into the cuboctahedral cavity. We illustrate this possibility by calculating the band structure of the hypothetical orthorhombic  $\text{CH}_3\text{NH}_3\text{BiAgCl}_6$  (constructed as described in the Supporting Information);

as expected we obtain a direct band gap, as shown in Figure S5.

Having established that the family of  $A_2BB'X_3$  halide double perovskites, based on  $B = \text{Sb}$ ,  $\text{Bi}$  and  $B' = \text{Cu}$ ,  $\text{Ag}$ ,  $\text{Au}$  exhibits promising optoelectronic properties, we move to the synthesis and optical characterization of a representative member of this group of compounds. We adapt the synthesis process of  $\text{Cs}_2\text{BiNaCl}_6$ , reported in Ref.,<sup>31</sup> to allow for the incorporation of a noble metal. Of the three noble metals under consideration,  $\text{Ag}$  has an ionic radius which is closest to that of  $\text{Na}$  ( $1.02 \text{ \AA}$  vs  $1.15 \text{ \AA}$ ). For this reason we proceed to synthesize  $\text{Cs}_2\text{BiAgCl}_6$  by conventional solid-state reaction as described in detail in the Supporting Information. In Figure 2a we show the X-ray Diffraction Pattern for a single crystal ( $\sim 30 \mu\text{m}$  diameter). We observe sharp reflections for the crystallographic  $0kl$ ,  $h0l$  and  $hk0$  planes. These reflections show characteristics of  $m\bar{3}m$  symmetry that reveal systematic absences for  $(hkl; h+k, k+l, h+l = 2n)$  corresponding to the face-centered space groups  $F432$ ,  $F\bar{4}3m$  and  $Fm\bar{3}m$ . The latter was selected for structure refinement after confirmation that  $\text{Cs}_2\text{BiAgCl}_6$  crystallizes in an FCC lattice. We find that there is no significant distortion of octahedral symmetry about the  $\text{Bi}^{3+}$ . The atomic positions from the structural refinement are listed in Table S2 of the Supplementary Information. The X-ray diffraction patterns uniquely identify the  $Fm\bar{3}m$  (no. 225) space group at room temperature, and the quantitative structural analysis gives a very good description of the data. In addition, our crystal structure refinement is consistent with the rock-salt configuration assumed by our atomistic model. The experimental and computationally predicted conventional lattice parameters are in very good agreement,  $10.78 \text{ \AA}$  and  $10.50 \text{ \AA}$ , respectively. From the optical absorption spectrum and Tauc plot (see Figure 2b) we can estimate an indirect optical band gap in the range of 2.3-2.5 eV. The indirect character of the band gap is consistent with the broad photoluminescence peak observed between 480 and 650 nm (1.9-2.6 eV) with the maximum at  $\sim 575 \text{ nm}$  (2.2 eV), red-shifted with respect to the optical absorption onset. In addition, the time-resolved photoluminescence decay shown in Figure 2c was fitted with a double exponential giving a fast component lifetime of 15 ns and a slow component lifetime of 100 ns.

In Figure 3 we show the electronic band structure of  $\text{Cs}_2\text{BiAgCl}_6$  calculated for the as deter-

mined experimental crystal structure, with and without relativistic spin-orbit coupling effects. The features of the valence band edge are almost unchanged when the relativistic effects are included. This is consistent with the predominant Cl-*p* and Ag-*d* character of this band. By contrast, due to the large spin-orbit coupling, the conduction band edge splits in two bands, separated by more than 1.5 eV at the  $\Gamma$  point. This effect is not surprising, given that the character of the conduction band bottom is of primarily Bi-*p* character. For comparison, in the case of Cs<sub>2</sub>SbAgCl<sub>6</sub> (see Figure S7) the spin-orbit splitting of the conduction band at the  $\Gamma$  point is of only 0.5 eV. The fundamental band gap is reduced by 0.4 eV upon inclusion of relativistic effects, and the shape of the conduction band is drastically different. Therefore, the inclusion of spin-orbit coupling is crucial for the correct description of the conduction band edge, bearing resemblance to the case of CH<sub>3</sub>NH<sub>3</sub>PbI<sub>3</sub>.<sup>32,33</sup> In the fully relativistic case we calculated an indirect band gap of 3.0 eV and lowest direct transition of 3.5 eV, in very close agreement with the results obtained for the model Cs<sub>2</sub>BiAgCl<sub>6</sub> structure, discussed in Figure 1 [2.7 eV (indirect) and 3.3 eV (direct)]. The small difference in band gap of 0.2-0.3 eV is due to the small difference in volume between the experimental and predicted crystal structure. The calculated electronic band gaps are overestimated with respect to the measured optical band gap by approximately 0.5 eV. This quantitative discrepancy does not affect the qualitative physical trends of the band gaps discussed throughout this work, and can be associated to the approximations employed in our PBE0 calculations. A better agreement with experiment can be reached by fine-tuning the fraction of exact exchange, or by performing *GW* calculations.<sup>34,35</sup> The latter will be reported in a future work.

In summary, through a combined theoretical and experimental study, we have designed a new family of halide double-perovskite semiconductors based on pnictogens and noble metals. These compounds have promising electronic properties, such as low carrier effective masses and band gaps covering the visible and near-infrared region of the optical spectrum. All compounds are indirect gap semiconductors and exhibit strong spin-orbit coupling. We successfully synthesized Cs<sub>2</sub>BiAgCl<sub>6</sub>, and obtained a face-centered cubic double perovskite, exhibiting optical properties consistent with an indirect gap semiconductor, in agreement with our computational predictions.

The present work is the first detailed description of the structure and optoelectronic properties of the pnictogen-noble metal halide double perovskite family, and calls for many future experimental and theoretical studies in order to assess the full potential of these new materials. We expect that a complete mapping of the genome of halide double perovskites based on pnictogens and noble metals may unlock a world of new exciting optoelectronic materials for solar cells, photodetectors, light-emitting devices, and transistors.

## **Acknowledgement**

The research leading to these results has received funding from the the Graphene Flagship (EU FP7 grant no. 604391), the Leverhulme Trust (Grant RL-2012-001), the UK Engineering and Physical Sciences Research Council (Grant No. EP/J009857/1 and EP/M020517/1), and the European Union Seventh Framework Programme (FP7/2007-2013) under grant agreements n°239578 (ALIGN) and n°604032 (MESO). The authors acknowledge the use of the University of Oxford Advanced Research Computing (ARC) facility (<http://dx.doi.org/10.5281/zenodo.22558>) and the ARCHER UK National Supercomputing Service under the ‘AMSEC’ Leadership project. G.V., M.R.F. and F.G. would like to thank Marios Zacharias for useful discussions. Figures involving atomic structures were rendered using VESTA.<sup>36</sup>

## **Note added**

During the preparation of this manuscript we became aware of the publication of two related papers: Ref.<sup>37</sup> (published February 7th, 2016) and Ref.<sup>38</sup> (published February 10th, 2016). The key difference between the present work and that of Ref.<sup>37,38</sup> is that we perform a computational screening of the entire family of pnictogen-noble metal double halide perovskites and perform experiments that confirm our predictions.



## References

- (1) Suntivich, J.; Gasteiger, H. A.; Yabuuchi, N.; Nakanishi, H.; Goodenough, J. B.; Shao-Horn, Y. Design principles for oxygen-reduction activity on perovskite oxide catalysts for fuel cells and metal-air batteries. *Nature Chemistry* **2011**, *3*, 546–550.
- (2) Stranks, S.; Snaith, H. J. Metal-Halide Perovskites for Photovoltaic and Light-Emitting Devices. *Nature Nanotechnology* **2015**, *10*, 391.
- (3) Grätzel, M. The Light and Shade of Perovskite Solar Cells. *Nature Materials* **2014**, *13*, 838.
- (4) Vasala, S.; Karppinen, M.  $A_2B\text{O}_6$  perovskites: A review. *Prog. Solid State Chem.* **2015**, *4*, 1–36.
- (5) Grinberg, L.; West, D. V.; Torres, M.; Gou, G.; Stein, D. M.; Wu, L.; Chen, G.; Gallo, E. M.; Akbashev, A. R.; Davies, P. K.; Spanier, J. E.; Rappe, A. M. Perovskite oxides for visible-light-absorbing ferroelectric and photovoltaic materials. *Nature* **2013**, *503*, 509–512.
- (6) Ramesh, R.; Spaldin, N. A. Multiferroics: progress and prospects in thin films. *Nature Mater.* **2007**, *6*, 21–29.
- (7) Rinjders, G.; Blank, D. H. A. Materials science: Build your own superlattice. *Nature* **2005**, *433*, 369–370.
- (8) Ahn, C. H.; Rabe, K. M.; Triscone, J.-M. Ferroelectricity at the Nanoscale: Local Polarization in Oxide Thin Films and Heterostructures. *Science* **2004**, *303*, 488–491.
- (9) Fan, Z.; Sun, K.; Wang, J. Perovskites for photovoltaics: a combined review of organic-inorganic halide perovskites and ferroelectric oxide perovskites. *J. Mater. Chem. A* **2015**, *3*, 18809.
- (10) Green, M.; Ho-Baillie, A.; Snaith, H. J. The Emergence of Perovskite Solar Cells. *Nature Photonics* **2014**, *8*, 506.

- (11) Lee, M. M.; Teuscher, J.; Miyasaka, T.; Myrakami, T. N.; Snaith, H. J. Efficient Hybrid Solar Cells Based on Meso-Superstructured Organometal Halide Perovskites. *Science* **2012**, *338*, 643.
- (12) Kim, H.-S.; Lee, C. R.; Im, J.-H.; Lee, K.-B.; Moehl, T.; Marchioro, A.; Moon, S.-J.; Humphry-Baker, R.; Yum, J.-H.; Moser, J. E.; M., G.; N.-G., P. Lead Iodide Perovskite Sensitized All-Solid-State Submicron Thin Film Mesoscopic Solar Cell with Efficiency Exceeding 9%. *Sci. Rep.* **2012**, *2*, 591.
- (13) Best Research-Cell Efficiencies. [http://www.nrel.gov/ncpv/images/efficiency\\_chart.jpg](http://www.nrel.gov/ncpv/images/efficiency_chart.jpg).
- (14) Manser, J. S.; Saidaminov, M. I.; Christians, J. A.; Bakr, O. M.; Kamat, P. V. Making and breaking of lead-halide perovskites. *Acc. Chem. Res.* **2016**,
- (15) Hoke, E. T.; Slotcavage, D. J.; Dohner, E. R.; Bowring, A. R.; Karunadasa, H. I.; McGehee, M. D. Reversible photo-induced trap formation in mixed-halide hybrid perovskites for photovoltaics. *Chem. Sci.* **2015**, *6*, 613–617.
- (16) Eames, C.; Frost, J. M.; Barnes, P. R. F.; O'Regan, A., B. C. and Walsh; Saiful Islam, M. Ionic transport in hybrid lead iodide perovskite solar cells. *Nature Commun.* **2015**, *6*, 7497.
- (17) Meloni, S.; Moehl, T.; Tress, W.; Grankvicius, M.; Saliba, M.; Hui, Y.; Gao, P.; Nazeeruddin, M. K.; Zakeeruddin, S. M.; Rothlisberger, U.; Grätzel, M. Ionic polarization induced current-voltage hysteresis in  $\text{CH}_3\text{NH}_3\text{PbX}_3$  perovskite solar cells. *Nature Commun.* **2016**, *7*, 10334.
- (18) Espinosa, N.; Serrano-Luján, L.; Urbina, A.; Krebs, F. C. Solution and Vapour Deposited Lead Perovskite Solar Cells: Ecotoxicity from a Life Cycle Assessment Perspective. *Solar Energy Materials and Solar Cells* **2015**, *137*, 303.

- (19) Babagayigit, A.; Thanh, D. D.; Ethirajan, A.; Manca, J.; Muller, M.; Boyen, H.-G.; Conings, B. Assessing the toxicity of Pb- and Sn-based perovskite solar cells in model organism *Danio rerio*. *Sci. Rep.* **2016**, *6*, 18721.
- (20) Stoumpos, C. C.; Malliakas, C. D.; Kanatzidis, M. G. Semiconducting Tin and Lead Iodide Perovskites with Organic Cations: Phase Transitions, High Mobilities, and Near-Infrared Photoluminescent Properties. *Inorg. Chem.* **2013**, *52*, 9019.
- (21) Baikie, T.; Fang, Y.; Kadro, J. M.; Schreyer, M.; Wei, F.; Mhaisalkar, S. G.; Grätzel, M.; White, T. J. Synthesis and Crystal Chemistry of the Hybrid Perovskite (CH<sub>3</sub>NH<sub>3</sub>PbI<sub>3</sub>) for Solid-State Sensitized Solar Applications. *J. Chem. Mater. A* **2013**, *1*, 5628.
- (22) Hao, F.; Stoumpos, C. C.; Cao, D. H.; Chang, R. P. H.; Kanatzidis, M. G. Lead-free Solid-State Organic-Inorganic Halide Perovskite Solar Cells. *Nature Photonics* **2014**, *8*, 489.
- (23) Noel, N.; Stranks, S. D.; Abate, A.; Wehrenfennig, C.; Guarnera, S.; Haghighirad, A.-A.; Sadhanala, A.; Eperon, G. E.; Pathak, S. K.; Johnston, A., M. B. andPetrozza; Herz, L. M.; Snaith, H. J. Lead-Free Organic-Inorganic Tin Halide Perovskite for Photovoltaic Applications. *Energ. Environ. Sci* **2014**, *7*, 3061.
- (24) Filip, M. R.; Giustino, F. Computational Screening of Homovalent Lead Substitution in Organic-Inorganic Halide Perovskites. *J. Phys. Chem. C* **2016**, *120*, 166–173.
- (25) Nechache, R. N.; Harnagea, C.; Li, S.; Cardenas, L.; Huang, W.; Chakrabarty, J.; Rosei, F. Bandgap tuning of multiferroic oxide solar cells. *Nature Photon.* **2015**, *9*, 61–67.
- (26) Berger, R. F.; Neaton, J. B. Computational design of low-band-gap double perovskites. *Phys. Rev. B* **2012**, *86*, 165211.
- (27) van Loef, E. V. D.; Dorenbos, P.; van Eijk, C. W. E.; Krämer, K. W.; Güdel, H. U. Scintillation and spectroscopy of the pure and Ce<sup>3+</sup>-doped elpasolites: Cs<sub>2</sub>LiYX<sub>6</sub> (X = Cl, Br). *J. Phys.: Condens. Matter.* **2002**, *14*, 8481–8496.

- (28) Shannon, R. D. Revised effective ionic radii and systematic studies of interatomic distances in halides and chalcogenides. *Acta. Cryst. A* **1976**, *32*, 751–767.
- (29) He, Y.; Galli, G. Perovskites for Solar Thermoelectric Applications: a First Principle Study of CH<sub>3</sub>NH<sub>3</sub>AI<sub>3</sub> (A = Pb and Sn). *Chem. Mater.* **2014**, *26*, 5394.
- (30) Filip, M. R.; Verdi, C.; Giustino, F. GW Band Structures and Carrier Effective Masses of CH<sub>3</sub>NH<sub>3</sub>PbI<sub>3</sub> and Hypothetical Perovskites of the Type APbI<sub>3</sub>: A = NH<sub>4</sub>, PH<sub>4</sub>, AsH<sub>4</sub> and SbH<sub>4</sub>. *J. Phys. Chem. C* **2015**, *119*, 25209–25219.
- (31) Morris, L. R.; Robinson, W. R. Crystal structure of Cs<sub>2</sub>BiNaCl<sub>6</sub>. *Acta Cryst. B* **1972**, *28*, 653–654.
- (32) Even, J.; Pedesseau, L.; Jancu, J.-M.; Katan, C. Importance of Spin-Orbit Coupling in Hybrid Organic/Inorganic Perovskites for Photovoltaic Applications. *J. Phys. Chem. Lett.* **2013**, *4*, 2999.
- (33) Filip, M. R.; Giustino, F. GW Quasiparticle Band Gap of the Hybrid Organic-Inorganic Perovskite CH<sub>3</sub>NH<sub>3</sub>PbI<sub>3</sub>: Effect of Spin-Orbit Interaction, Semicore Electrons, and Self-Consistency. *Phys. Rev. B* **2014**, *90*, 245145.
- (34) Hedin, L. New Method for Calculating the One-Particle Green's Function with Application to the Electron-Gas Problem. *Phys. Rev.* **1965**, *139*, A796.
- (35) Hybertsen, M. S.; Louie, S. G. Electron Correlation in Semiconductors and Insulators: Band Gaps and Quasiparticle Energies. *Phys. Rev. B* **1986**, *34*, 5390.
- (36) Momma, K.; Izumi, F. VESTA: A Three-Dimensional Visualization System for Electronic and Structural Analysis. *J. Appl. Cryst.* **2008**, *41*, 653.
- (37) Slavney, A. H.; Hu, T.; Lindenberg, A. M.; Karunadasa, H. I. A Bismuth-Halide Double Perovskite with Long Carrier Recombination Lifetime for Photovoltaic Applications. *J. Am. Chem. Soc.* **2016**, *139*.

(38) McClure, E. T.; Ball, M. R.; Windl, W.; Woodward, P. M. Cs<sub>2</sub>AgBiX<sub>6</sub> (X = Br, Cl): New visible light absorbing, lead-free halide perovskite semiconductors. *Chem. Mater.* **2016**,

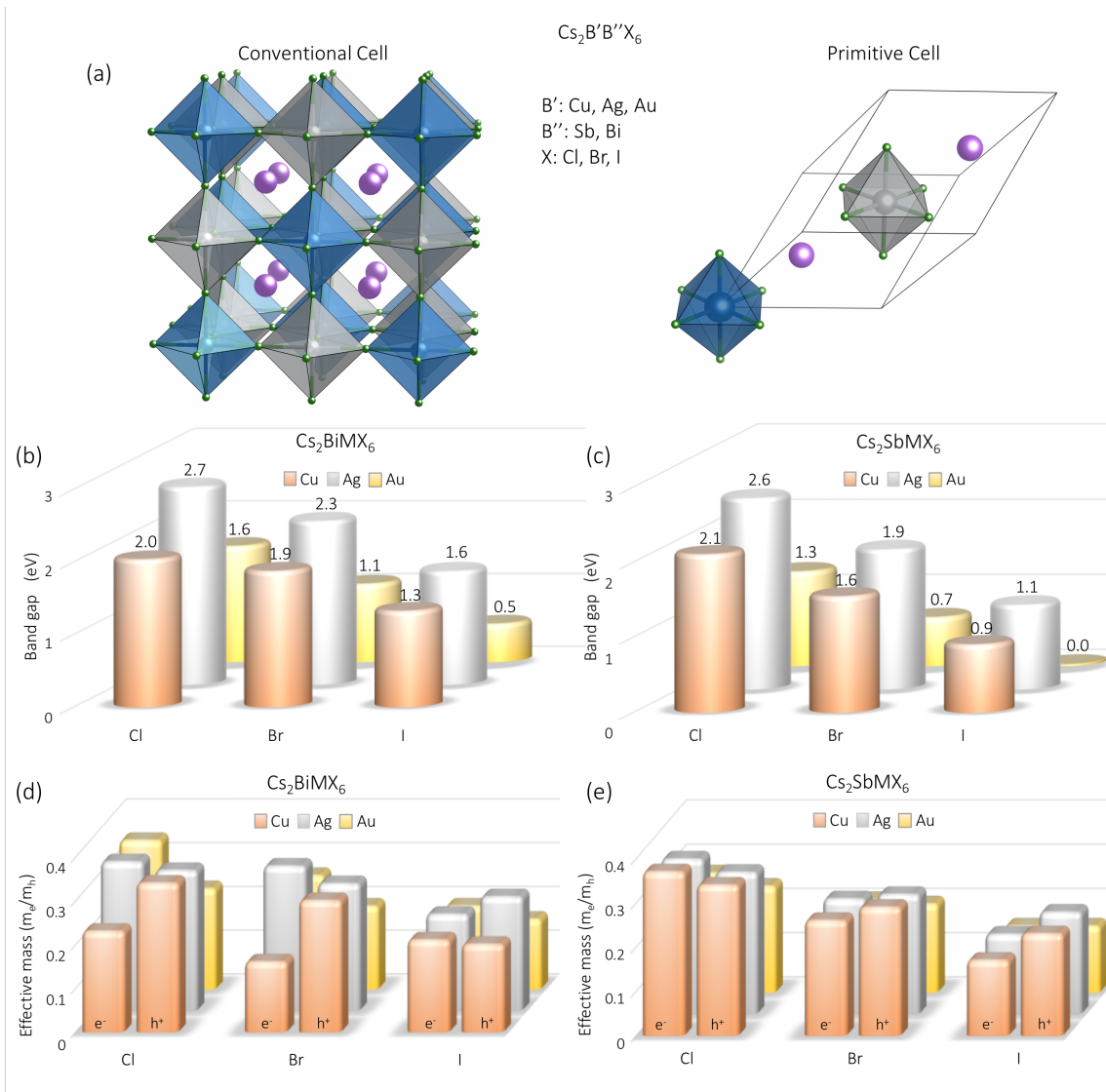


**Figure 1: Computational screening of the electronic properties of the pnictogen-noble metal halide double perovskites**

**a** Polyhedral model of the conventional (left) and reduced (right) unit cell of the hypothetical halide double perovskites. The pnictogen (B') and noble metal (B'') cations alternate along the three crystallographic axes, forming the rock-salt ordering. **b** Electronic band gaps calculated for all compounds in the halide double perovskite family using the PBE0 hybrid functionals. All calculated band gaps are indirect with the top of the valence band at the X point  $(0,0,2\pi/a)$  of the Brillouin zone, where  $a$  is the lattice parameter of the FCC unit cell. The bottom of the conduction band is at the L point  $(\pi/a, \pi/a, \pi/a)$  of the Brillouin zone in all cases, except  $\text{Cs}_2\text{BiAgCl}_6$ ,  $\text{Cs}_2\text{BiCuCl}_6$  and  $\text{Cs}_2\text{BiCuBr}_6$  where the bottom of the conduction band is found at the  $\Gamma$   $(0,0,0)$  point. **c** Transport effective masses calculated from DFT/LDA for each compound (see Supporting Information). The effective masses are calculated at the VBM (holes) and CBM (electrons) in each case.

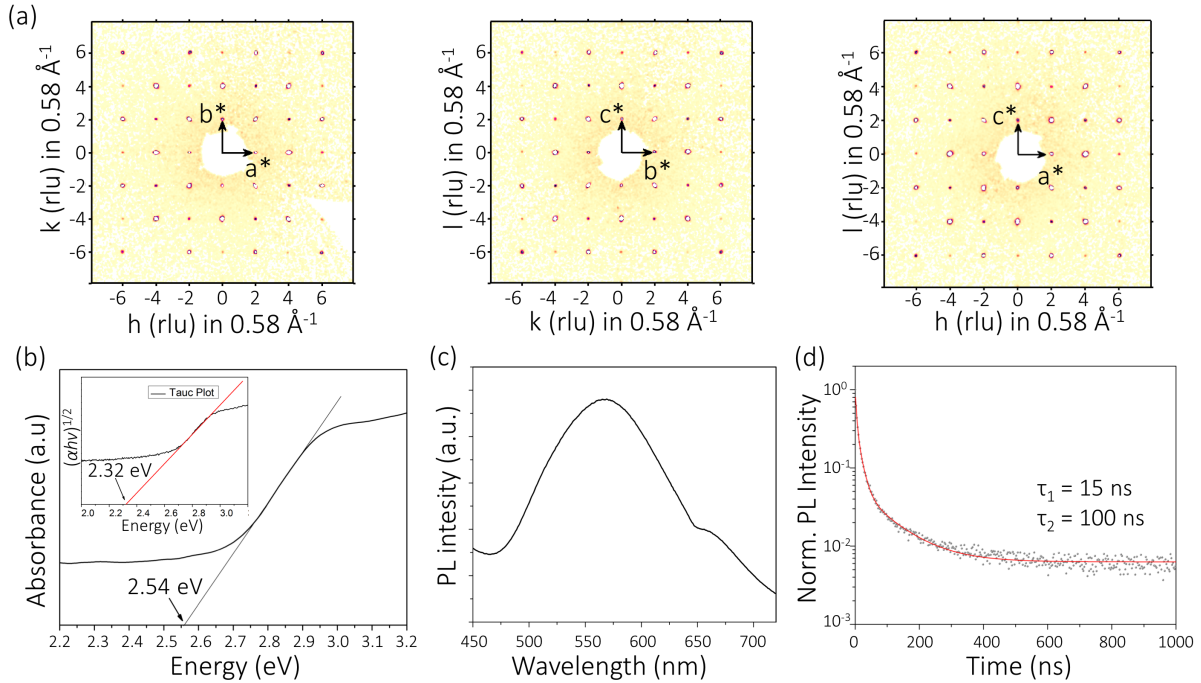


**Figure 2: Experimental synthesis and characterization of  $\text{Cs}_2\text{BiAgCl}_6$ .**

**a** X-ray diffraction pattern for a  $\text{Cs}_2\text{BiAgCl}_6$  single crystal at 293 K.  $hkl$  shown for three different planes, i.e.  $0kl$ ,  $h0l$  and  $hk0$ . All wave vectors are labeled in reciprocal lattice units (rlu) and  $a^*$ ,  $b^*$  and  $c^*$  denote reciprocal lattice vectors of the cubic cell of the  $Fm\bar{3}m$  structure. **b** UV-Vis optical absorption spectrum of  $\text{Cs}_2\text{BiAgCl}_6$ . The inset shows the Tauc plot, corresponding to an indirect allowed transition [assuming the expression:  $(\alpha hv)^{1/2} = C(hv - E_g)$ , where  $\alpha$  is the absorption coefficient,  $hv$  is the energy of the incoming photon  $E_g$  is the optical band gap and  $C$  is a constant]. The straight lines are fitted to the linear regions of the absorption spectrum and Tauc plot, and the intercepts at 2.32 eV and 2.54 eV marked on the plot are calculated from the fit. **c** Steady-state photoluminescence (PL) spectrum of  $\text{Cs}_2\text{BiAgCl}_6$ , deposited on glass. **d** Time resolved photoluminescence decay of  $\text{Cs}_2\text{BiAgCl}_6$ , deposited on glass. The data is fitted using a biexponential decay function. The decay lifetimes of 15 ns (fast) and 100 ns (slow) is estimated from the fit.

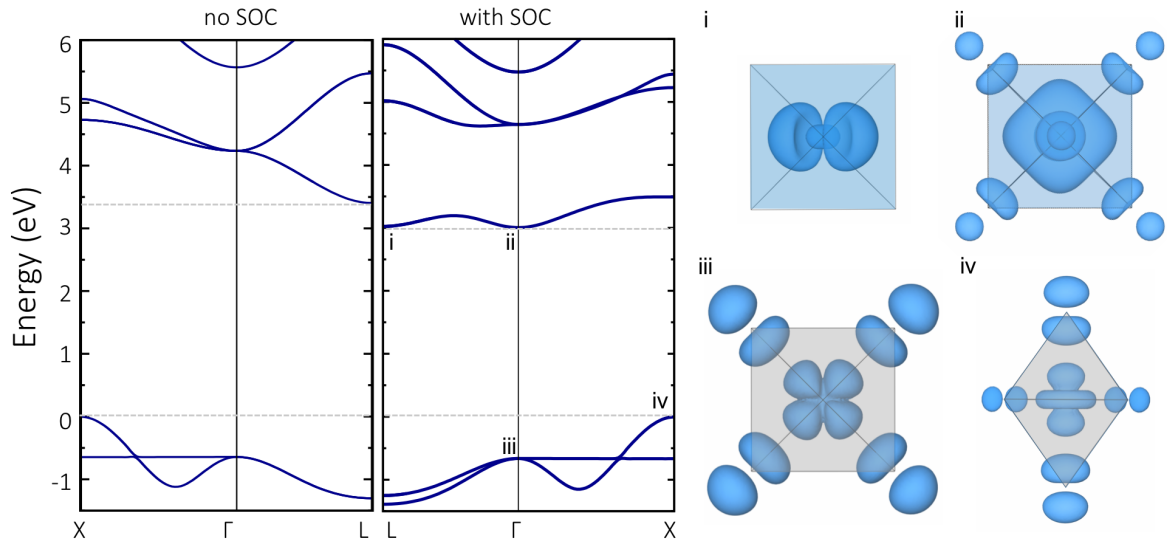


Figure 3: **Electronic structure properties calculated for the experimental crystal structure of  $\text{Cs}_2\text{BiAgCl}_6$ .**

The Band structure of  $\text{Cs}_2\text{BiAgCl}_6$  calculated along the high symmetry path  $L(\pi/a, \pi/a, \pi/a) - \Gamma(0,0,0) - X(0,0,2\pi/a)$  without (left) and with (right) spin-orbit coupling. The black points on the fully relativistic band structure marked 'i-iv' mark the conduction band bottom at L and  $\Gamma$  and the valence band top at  $\Gamma$  and X, respectively. For each of the states we show the electronic wavefunctions. The conduction band bottom is primarily of Bi- $p$  and Cl- $p$  character, while the valence band top consists of Ag- $d$  and Cl- $p$  character. The shape of all four wavefunctions is consistent with metal-halide  $\sigma$ -bonds.